Fractality in complex networks: Critical and supercritical skeletons

J. S. Kim,[1] K.-I. Goh,[2] G. Salvi,[1] E. Oh,[1] B. Kahng,[1,3] and D. Kim[1]

[1]*CTP and FPRD, School of Physics and Astronomy, Seoul National University, Seoul 151-747, Korea*
[2]*Center for Complex Network Research and Department of Physics, University of Notre Dame, Notre Dame, Indiana 46556, USA*
and Department of Physics, Korea University, Seoul 136-713, Korea
[3]*Center for Nonlinear Studies, Los Alamos National Laboratory, Los Alamos, New Mexico 87545, USA*

Fractal scaling—a power-law behavior of the number of boxes needed to tile a given network with respect to the lateral size of the box—is studied. We introduce a box-covering algorithm that is a modified version of the original algorithm introduced by Song *et al.* [Nature (London) **433**, 392 (2005)]; this algorithm enables easy implementation. Fractal networks are viewed as comprising a skeleton and shortcuts. The skeleton, embedded underneath the original network, is a special type of spanning tree based on the edge betweenness centrality; it provides a scaffold for the fractality of the network. When the skeleton is regarded as a branching tree, it exhibits a plateau in the mean branching number as a function of the distance from a root. For nonfractal networks, on the other hand, the mean branching number decays to zero without forming a plateau. Based on these observations, we construct a fractal network model by combining a random branching tree and local shortcuts. The scaffold branching tree can be either critical or supercritical, depending on the small worldness of a given network. For the network constructed from the critical (supercritical) branching tree, the average number of vertices within a given box grows with the lateral size of the box according to a power-law (an exponential) form in the cluster-growing method. The critical and supercritical skeletons are observed in protein interaction networks and the World Wide Web, respectively. The distribution of box masses, i.e., the number of vertices within each box, follows a power law $P_m(M) \sim M^{-\eta}$. The exponent η depends on the box lateral size ℓ_B. For small values of ℓ_B, η is equal to the degree exponent γ of a given scale-free network, whereas η approaches the exponent $\tau = \gamma/(\gamma-1)$ as ℓ_B increases, which is the exponent of the cluster-size distribution of the random branching tree. Finally, we study the perimeter H_α of a given box α, i.e., the number of edges connected to different boxes from a given box α as a function of the box mass $M_{B,\alpha}$. It is obtained that the average perimeter over the boxes with box mass M_B is likely to scale as $\langle H(M_B) \rangle \sim M_B$, irrespective of the box size ℓ_B.

I. INTRODUCTION

Fractal scaling recently observed [1] in real-world scale-free (SF) networks such as the World Wide Web (WWW) [2], metabolic network of *Escherichia coli* and other microorganisms [3], and protein interaction network of *Homo sapiens* [4] has opened a new perspective in the study of networks. SF networks [5] are those that exhibit a power-law degree distribution $P_d(k) \sim k^{-\gamma}$. Degree k is the number of edges connected to a given vertex. Fractal scaling implies a power-law relationship between the minimum number of boxes $N_B(\ell_B)$ needed to tile the entire network and the lateral size of the boxes ℓ_B, i.e.,

$$N_B(\ell_B) \sim \ell_B^{-d_B}, \tag{1}$$

where d_B is the fractal dimension [6]. This power-law scaling implies that the average number of vertices $\langle M_B(\ell_B) \rangle$ within a box of lateral box size ℓ_B scales according to a power law as

$$\langle M_B(\ell_B) \rangle \sim \ell_B^{d_B}. \tag{2}$$

Here, the relation of system size $N \sim N_B(\ell_B)\langle M_B(\ell_B)\rangle$ is used. This counting method is called the box-covering method. At a glance, the power-law fractal scaling (1) is not consistent with the notion of small worldness (SW) of SF

networks. SW implies that the average number of vertices within a distance ℓ_C from a vertex scales as

$$\langle M_C(\ell_C) \rangle \sim e^{\ell_C/\ell_0}, \tag{3}$$

where ℓ_0 is a constant. This counting method is called the cluster-growing method. Here, subscripts B and C represent the box-covering and cluster-growing methods, respectively. The number of vertices M within a box is referred to as the box mass. This contradiction can be resolved by the fact that a vertex is (can be) counted only once (more than once) in the box-covering method (in the cluster-growing method).

Recently, it was suggested that the fractal scaling originates from the disassortative correlation between two neighboring degrees [7] or the repulsion between hubs [8]. Moreover, we showed [9] that the fractal network contains the fractal skeleton [10] underneath it; this skeleton is a special type of spanning tree, formed by edges with the highest betweenness centralities [11,12] or loads [13]. The remaining edges in the network are referred to as shortcuts that contribute to loop formation. The skeleton of a SF network also follows a power-law degree distribution, where its degree exponent can differ slightly from that of the original network [10]. For fractal networks that follow fractal scaling (1), we have shown [9] that each of their skeletons exhibits fractal scaling similar to that of the original network. The number of boxes needed to cover the original network is almost identi-

cal to that needed to cover the skeleton. Thus, since the skeleton is a simple tree structure, it is more useful than the original network for studying the origin of the fractality.

It was shown [9] that the skeleton of the fractal network exhibits a nondying branching structure, referred to as a *persistent* branching structure hereafter. A skeleton can be considered as a tree generated in a branching process [14] starting from the root vertex. This mapping can be applied to any tree. If a branching process occurs in an uncorrelated manner, the branching tree obtained from it exhibits a plateau, albeit fluctuating, in the mean branching number function $\bar{n}(d)$, which is defined as the average number of offsprings created by vertices at a distance d from the root. Actually, the plateau is formed when $\bar{n}(d)$ is independent of d; this is denoted as $\bar{n}$ for future discussions. The branching tree structure obtained from the random branching process is known to be a fractal for the critical case [15,16], where the mean branching rate is $\langle n \rangle = 1$. Here, $\langle n \rangle$ is defined as

$$\langle n \rangle \equiv \sum_{n=0}^{\infty} n b_n, \qquad (4)$$

where b_n is the probability that a vertex will produce n offsprings in each step. Thus, $\langle n \rangle = \bar{n}$ for the random branching tree. The fractal dimension of the SF branching tree generated with branching probability $b_n \sim n^{-\gamma}$ is given by [15–17]

$$d_B = \begin{cases} (\gamma-1)/(\gamma-2) & \text{for } 2 < \gamma < 3, \\ 2 & \text{for } \gamma > 3. \end{cases} \qquad (5)$$

Thus, the presence of the skeleton as the critical branching tree served as a scaffold for the fractality of the fractal network. Then, the original fractal network is a dressed structure to the skeleton with local shortcuts; the number of shortcuts is kept minimal in order to ensure fractality. This idea is demonstrated by observing that the number of boxes in the fractal scaling (1) for an original fractal network is similar to that of its skeleton [9]. When $\langle n \rangle > 1$, we will show that a supercritical branching tree is also a fractal from the perspective of the fractal scaling (1), although exponential relation in the average box mass (3) holds in the cluster-growing method. The supercritical branching tree also exhibits a plateau in $\bar{n}(d)$. Based on these observations, we define a network to be a fractal if (i) it exhibits a power-law scaling Eq. (1) in the box-covering method *and* (ii) its skeleton is also a fractal with the persistent branching structure, i.e., a plateau exists in the mean branching number function $\bar{n}(d)$.

Based on these findings, we introduced a fractal network model by incorporating the random critical branching tree and local shortcuts [9]. In this paper, we will show that the model can also be generalized for the supercritical branching tree, thereby facilitating a better understanding of fractal networks. For example, the model based on the supercritical branching tree can explain the subtle coexistence of SW and fractality as observed in the WWW.

Due to the heterogeneity of the degree distribution in the SF networks, the distribution of box masses is also nontrivial. It exhibits a power-law tail with exponent η,

$$P_m(M_B) \sim M_B^{-\eta}, \qquad (6)$$

in the box-covering method, whereas it exhibits a peak at a characteristic mass in the cluster-growing method. In this paper, we perform a detailed analysis of the real-world fractal network as well as the fractal network model, thereby showing that the box-mass distribution in the box-covering method for the fractal network can be explained by the branching dynamics. The exponent η of the box mass distribution is related to the exponent τ that describes the size distribution of random branching trees [14]. In particular, for the critical SF branching tree, τ is known to be [16–18]

$$\tau = \begin{cases} \gamma/(\gamma-1) & \text{for } 2 < \gamma < 3, \\ 3/2 & \text{for } \gamma > 3. \end{cases} \qquad (7)$$

The same value of τ can be derived for the supercritical SF branching tree; however, the power-law scaling behavior is limited to a finite characteristic size depending on $\langle n \rangle$ and γ [19]. Thus, the cluster-size distribution follows a power law for both the critical branching tree and the supercritical branching tree up to the characteristic size.

In the first part of this paper, we present the fractal property of real-world networks and the model of the fractal network in detail as well as a further analysis of our previous work [9]. Initially, in Sec. II we introduce a modified version of the box-covering method employed in this paper, following which we present the fractal scaling (Sec. III) and the mean branching number analysis (Sec. IV) for an extended list of complex networks, real-world and model networks. In the latter part, we provide a general description of a model of fractal SF networks including the supercritical branching tree and study its property in detail in Sec. V. In Sec. VI, we examine the average box mass and the box mass distribution for the fractal networks in the box-covering and cluster-growing methods. The average perimeter of a box as a function of the box mass is studied in Sec. VII. The summary follows in Sec. VIII.

II. THE BOX-COVERING METHOD

The fundamental relation of fractal scaling (1) is based on the procedure referred to as the box-covering method [1] that calculates the number of boxes N_B needed to cover the entire network with boxes of lateral size ℓ_B. This is analogous to the box-counting method normally used in fractal geometry [6]. Song *et al.* [1] introduced a new definition of the box applicable to complex networks such that the maximum separation between any pair of vertices within each box is less than ℓ_S. However, this particular definition has proved to be inessential for fractal scaling. Since ℓ_B (ℓ_S) can be regarded as the radius (diameter) of a box, a simple relation $\ell_S = 2\ell_B + 1$ would follow. This relation, however, turns out to be only approximate, and more understanding of the relationship is needed. Throughout this study, we utilize a different version of the box-covering method introduced here; this method involves sequential steps of box covering, thereby providing an easy implementation:

(i) Select a vertex randomly at each step; this vertex serves as a seed.
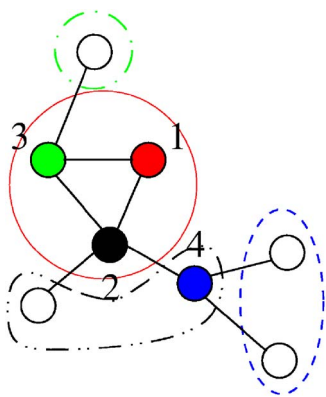
FIG. 1. (Color online) Schematic illustration of the box-covering algorithm introduced in this work. Vertices are selected randomly, for example, from vertex 1 to 4 successively. Vertices within distance $\ell_B=1$ from vertex 1 are assigned to a box represented by a solid (red) circle. Vertices from vertex 2, not yet assigned to their respective box, are represented by a dashed-dotted-dotted (black) closed curve, vertices from vertex 3 are represented by a dashed-dotted (green) circle, and vertices from vertex 4 are represented by dashed (blue) ellipse.

(ii) Search the network by distance ℓ_B from the seed and assign *newly burned vertices* to the new box. If no new vertex is found, do nothing.

(iii) Repeat (i) and (ii) until all vertices are assigned to their respective boxes.

The above method is schematically illustrated in Fig. 1. It should be noted that vertices can be disconnected within a box, but connected through a vertex (or vertices) in a different box (or boxes) as in the case of box 2 as shown in Fig. 1. On the other hand, if we construct a box with only connected vertices, the power-law behavior Eq. (1) is not observed. It is not obvious whether such behavior is intrinsic or algorithm dependent. A different Monte Carlo realization of this procedure [(i)–(iii)] yields a different number of boxes for covering the network. In this study, for simplicity, we choose the smallest number of boxes among all the trials. To obtain the power-law behavior of the fractal scaling, we needed at most $O(10)$ Monte Carlo trials for all fractal networks. Although this algorithm provides equivalent fractal dimension d_B to the one introduced by Song *et al.* [1], it is easier to implement. However, the algorithm in Ref. [1] can generate smaller number of boxes needed to tile a given network compared with ours. In Fig. 2, we compare the two box-covering methods applied to the WWW, demonstrating that the same fractal dimension d_B is obtained. It should be noted that the box number N_B we employ is not the *minimum* number among all the possible tiling configurations. Finding the actual minimum number over all configurations is a challenging task, which could not be reached by the Monte Carlo method. However, in this paper, we focus on the problem of the fractal scaling within the framework of the box-covering algorithm introduced above.

III. FRACTAL SCALING ANALYSIS

We present fractal scaling analysis for real-world networks, which are listed in the left column of Fig. 3. We first
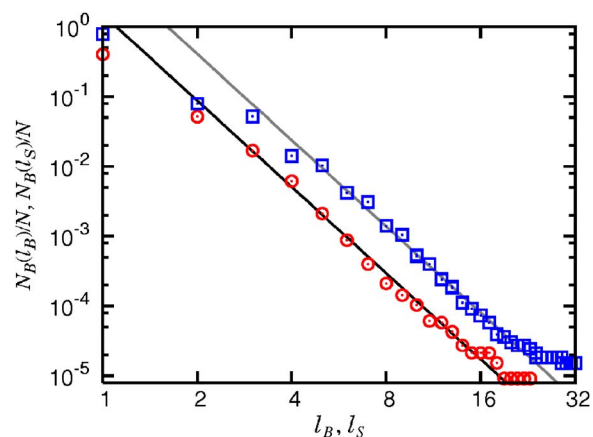

FIG. 2. (Color online) Comparison of the box-covering methods introduced by Song *et al.* [1] ($\square$) and in this paper ($\bigcirc$) for the WWW. The results obtained from the two box-covering methods applied to the WWW are plotted here. The two methods yield the same fractal dimension $d_B \approx 4.1$.

examine fractal networks such as (a) the World Wide Web, (b) the metabolic network of *E. coli*, (c) protein interaction network (PIN) of *H. sapiens*, and (d) of *S. cerevisiae* [20]. Next, nonfractal networks such as (e) the actor network [21], (f) coauthorship network [22], (g) Internet at the autonomous system (AS) level [23], (h) Internet at the router level [24], and (i) power grid of the USA [25] are studied. The characteristics of these networks are listed in Table I. Note that in the previous study by Song *et al.*, the protein interaction network of *S. cerevisiae* was classified as a nonfractal network. In this work, we use a different dataset [20] of high-confidence protein interactions, for which the PIN is a fractal network.

For the fractal networks (a)–(d), the original network and its skeleton exhibit the same fractal scaling behavior, and the respective statistics of the numbers of boxes needed to cover them are almost identical as shown in the left-hand column of Figs. 3(a)–3(d). The fractal dimensions for these networks are measured to be $\approx 4.10 \pm 0.12$, 3.53 ± 0.12, 2.28 ± 0.11, and 2.01 ± 0.15 for (a) the WWW, (b) the metabolic network, (c) PIN of human, and (d) that of yeast, respectively. A power-law behavior is not observed for nonfractal networks, in which $N_B(\ell_B)$ decays faster than any power law. We also study the fractal scaling for a random spanning tree of each network, which is constructed from edges that are randomly selected from the original network to form a tree. Since edges are selected randomly, the degree distribution of the original network is conserved in the random spanning tree. The random spanning tree is fractal irrespective of the fractality of the original networks; this follows from the percolation theory [26,27]. Thus, the random spanning tree is expected to follow a power law asymptotically in the fractal scaling, even though the numerical data for some examples may not show the power-law behavior clearly due to the finite-size effect. The fractal dimensions for the random spanning trees measured in asymptotic the regime are $\approx 3.76 \pm 0.06$ for (a), 3.94 ± 0.16 for (b), 2.24 ± 0.18 for (c), 1.84 ± 0.04 for (d), 2.91 ± 0.03 for (e), 2.68 ± 0.07 for (f), 2.76 ± 0.09 for (g), 3.37 ± 0.04 for (h), and 2.44 ± 0.07 for (i).
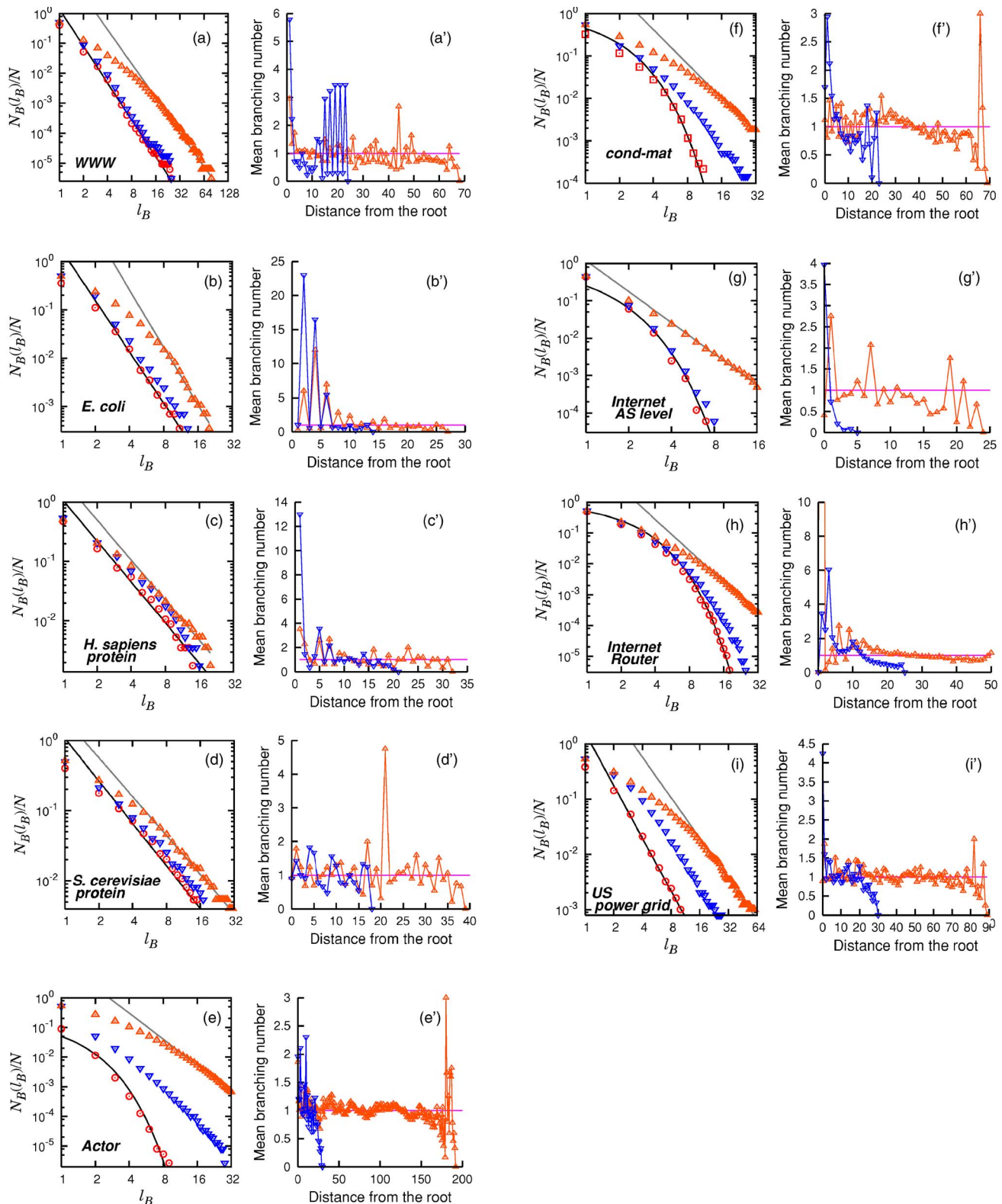
FIG. 3. (Color online) Fractal scaling analysis (left-hand column) and mean branching number (right-hand column) of real-world networks including fractal (a)–(d) and nonfractal (e)–(i) networks. For each network, the original network ($\bigcirc$), the skeleton ($\triangledown$), and a random spanning tree ($\triangle$) are studied. In (a)–(d), the straight lines, drawn for guidance, have slopes of −4.10, −3.53, −2.28, and −2.01, respectively, for the original networks. Those for the random spanning trees have slopes of −3.76, −3.94, −2.24, and −1.84. In (e)–(h), the fits to the exponential function for the original network and to a power-law function for the random spanning tree are shown. In the right-hand panels (a′)–(i′), the horizontal line at 1 is drawn for reference.

TABLE I. Properties of real-world networks studied in this work. For each network, the number of vertices N, the average degree $\langle k \rangle$, the assortativity mixing index r, the average separation $\langle d \rangle$ of all pairs of vertices, and the maximum separation d_{max} among all pairs of vertices are tabulated.

Name	N	$\langle k \rangle$	r	$\langle d \rangle$	d_{max}	Category
World Wide Web	325729	6.7	−0.05	7.2	46	Fractal and SW
Metabolic network of *E. coli*	2859	4.8	−0.16	4.7	18	Fractal and SW
PIN of *H. sapiens*	563	3.1	−0.14	6.9	21	Fractal but not SW
PIN of *S. cerevisiae*	741	4.7	−0.41	10.8	27	Fractal but not SW
Actor network	374511	80.2	−0.22	3.7		Nonfractal and SW
Coauthorship network (cond-mat)	13861	6.4	−0.16	6.6	18	Nonfractal and SW
Internet at the AS level	16644	4.3	−0.20	3.7	10	Nonfractal and SW
Router network	284805	3.2	−0.01	8.8	30	Nonfractal and SW
Power grid of the USA	4941	4.9	−0.06	8.5	17	Undetermined and SW

For nonfractal networks, the box number N_B does not follow a power law with respect to the box lateral size ℓ_B. The statistics of box number of skeletons differ significantly from those of their original network; however, there are some exceptions in our examination. For the Internet at the AS level

[Fig. 3(g)], N_B for the original network and skeleton exhibits similar behavior; however, they do not follow a power law. On the other hand, in the power grid [Fig. 3(i)], the fractal scalings of the original network and the skeleton exhibit the same power-law exponent; however, the box numbers for the
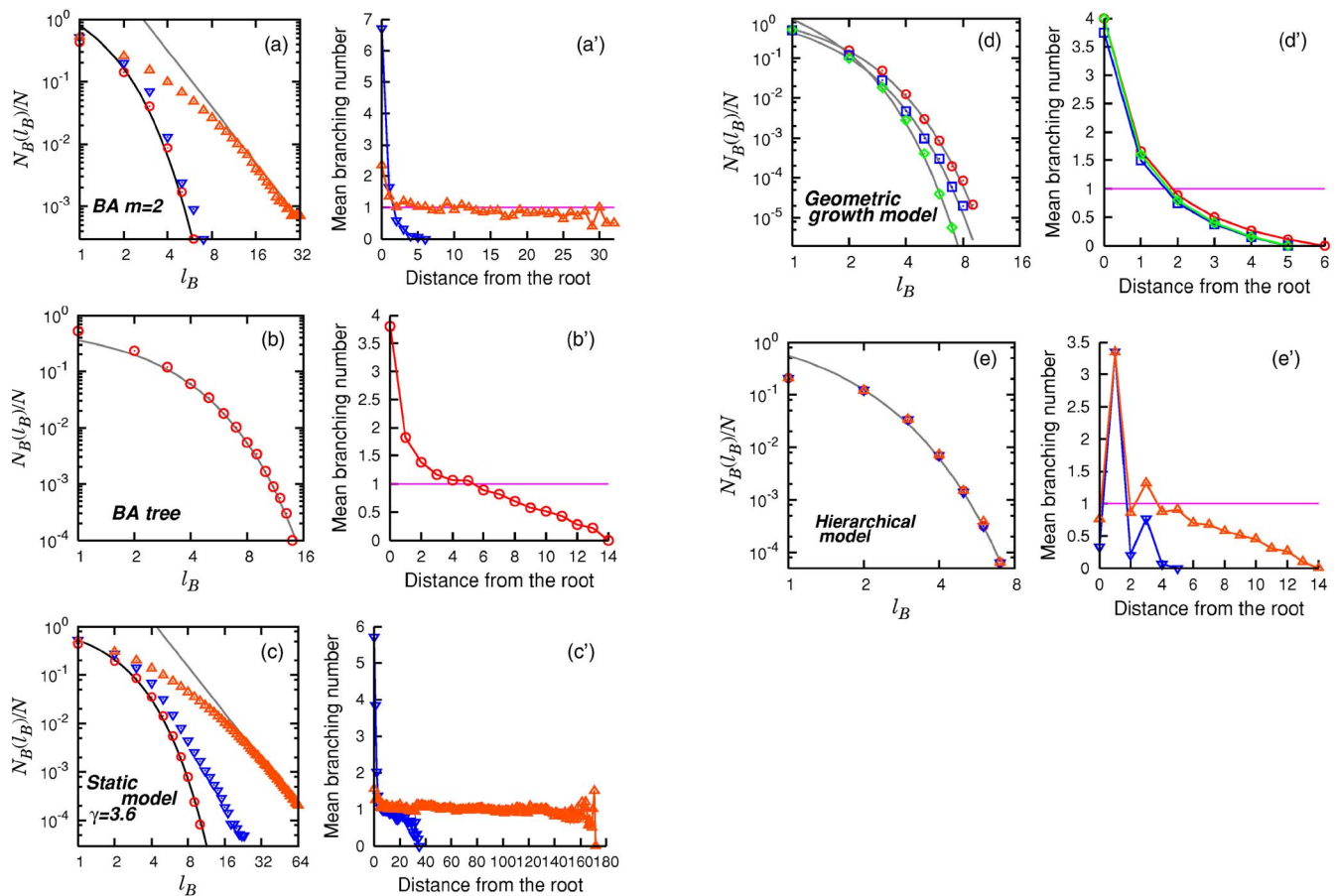

FIG. 4. (Color online) Fractal scaling analysis (a)–(e) and mean branching number (a′)–(e′) of the SF network models. The symbols used are similar to those in Fig. 3 except in (d). The different symbols in (d) represent different parameters in the model. Red circle, blue square, and green diamond symbols represent generations $m=1$, 2, and 3 of the model, respectively. In (a) and (c), the exponential fit for the original network and a power-law fit for the random spanning tree are shown. For (b) and (d), which are tree networks, the exponential fit is shown. In (e), the exponential fit for the original network is shown. Note that in (e), the box numbers for the original network, the skeleton, and the random spanning tree all overlap. In panels (a′)–(e′), a horizontal line at 1 is drawn for reference.

original network and the skeleton differ significantly. Although the fractal scaling exhibits a power-law behavior, this fractality is not obvious, because the network size is too small for checking if a plateau is intrinsically formed in $\bar{n}(d)$. Thus, the fractality cannot be classified.

Next, we examine fractal scaling in the following network models: (a) the Barabási-Albert model with the degree of incident vertex $m=2$ [5], (b) Barabási-Albert model tree with $m=1$, (c) static model [13], (d) geometric growth model [28], and (e) deterministic hierarchical model [29] in Fig. 4. The network models considered do not obey the power-law fractal scaling; therefore, they are not fractals.

IV. MEAN BRANCHING NUMBER ANALYSIS

We present the mean branching number (MBN) analysis for the skeleton and random spanning trees of each network considered. We define the MBN function $\bar{n}(d)$ as the mean number of offsprings of each vertex at distance d from the root in a branching tree. For the fractal networks [Figs. 3(a')–3(d')], both the skeleton and the random spanning tree exhibit a plateau in MBN, a signature of a persistent branching structure. For random spanning trees, the location of the plateau is distinctly obtained as $\bar{n} \approx 1$. With regard to the skeletons, while the plateaus in MBN of the protein interaction networks [Figs. 3(c')–3(d')] appear to be located around $\bar{n} \approx 1$, they cannot be located clearly for the WWW and metabolic network due to large fluctuations [Figs. 3(a')–3(b')]. Such fluctuations may originate due to various factors such as the finite-size effect and the artificial choice of the root of the branching tree. The dynamic origin of the formation of real-world networks may well be more complicated than the purely random branching dynamics: Thus, nontrivial correlations may exist. Although the location of the plateau in MBN cannot be clearly determined in some cases, its presence is a distinct feature of the fractal networks and is absent in nonfractal networks.

For nonfractal networks, the MBN of the skeleton decays to zero without forming a plateau [Figs. 3(e')–3(h')]. This is because the skeleton of each nonfractal SF network belongs to the class of "causal" trees [30], where vertices closer to the root are likely to have larger degrees. In such structures, MBN decreases steadily with the distance from the root; therefore, a plateau cannot be formed. This absence of a plateau in MBN is also observed in the skeletons of the network models shown in Fig. 4. Note that even for nonfractal networks, the random spanning trees exhibit plateaus at $\bar{n} \approx 1$, confirming their fractality independent of the underlying original network structure.

Although the fractal skeleton provides a scaffold for fractality in fractal networks, the manner in which the shortcuts are placed in the network is also important for preserving the fractality. With regard to this, the previous result of the length distribution of shortcuts [10] is important. It is known that two types of shortcut length distributions exist [10]. In the first type, the shortcut length distribution decays all the way with respect to the shortcut length. In the other type, the shortcut length distribution exhibits a peak at a finite length, which is comparable to the average separation of all pairs of
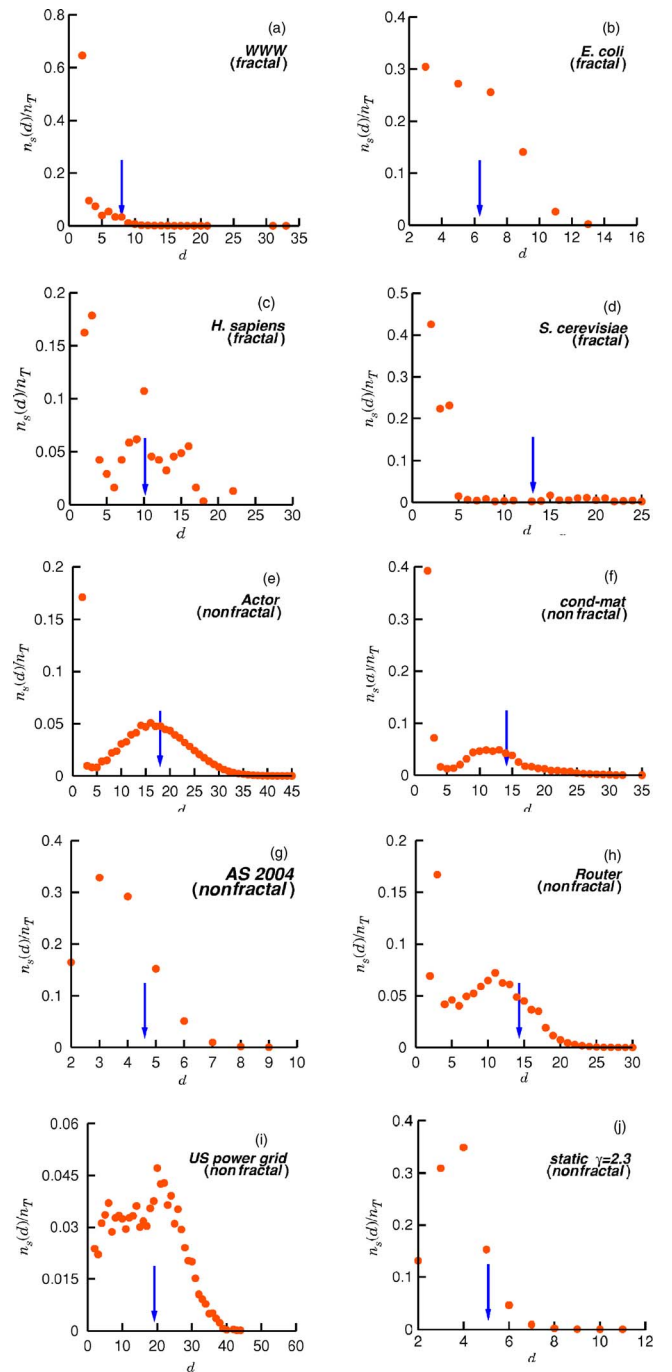

FIG. 5. (Color online) Length distribution of shortcuts. The length of a shortcut is defined as the shortest distance along the skeleton between the two vertices connected by the shortcut. The arrows indicate the diameter of the skeleton of each network. Here, $n_s(d)$ and n_T are the number of shortcuts with length d and the total number of shortcuts, respectively.

vertices on each skeleton; this is indicated by an arrow for each network in Fig. 5. Thus, in the former case, the shortcuts connecting different branches of the skeleton are rare; however, their contribution is considerable in the latter case. In the latter case, the network will be globally interwoven and loses the fractality as in the case of random SF networks. Indeed, we have found that the fractal networks exhibit the
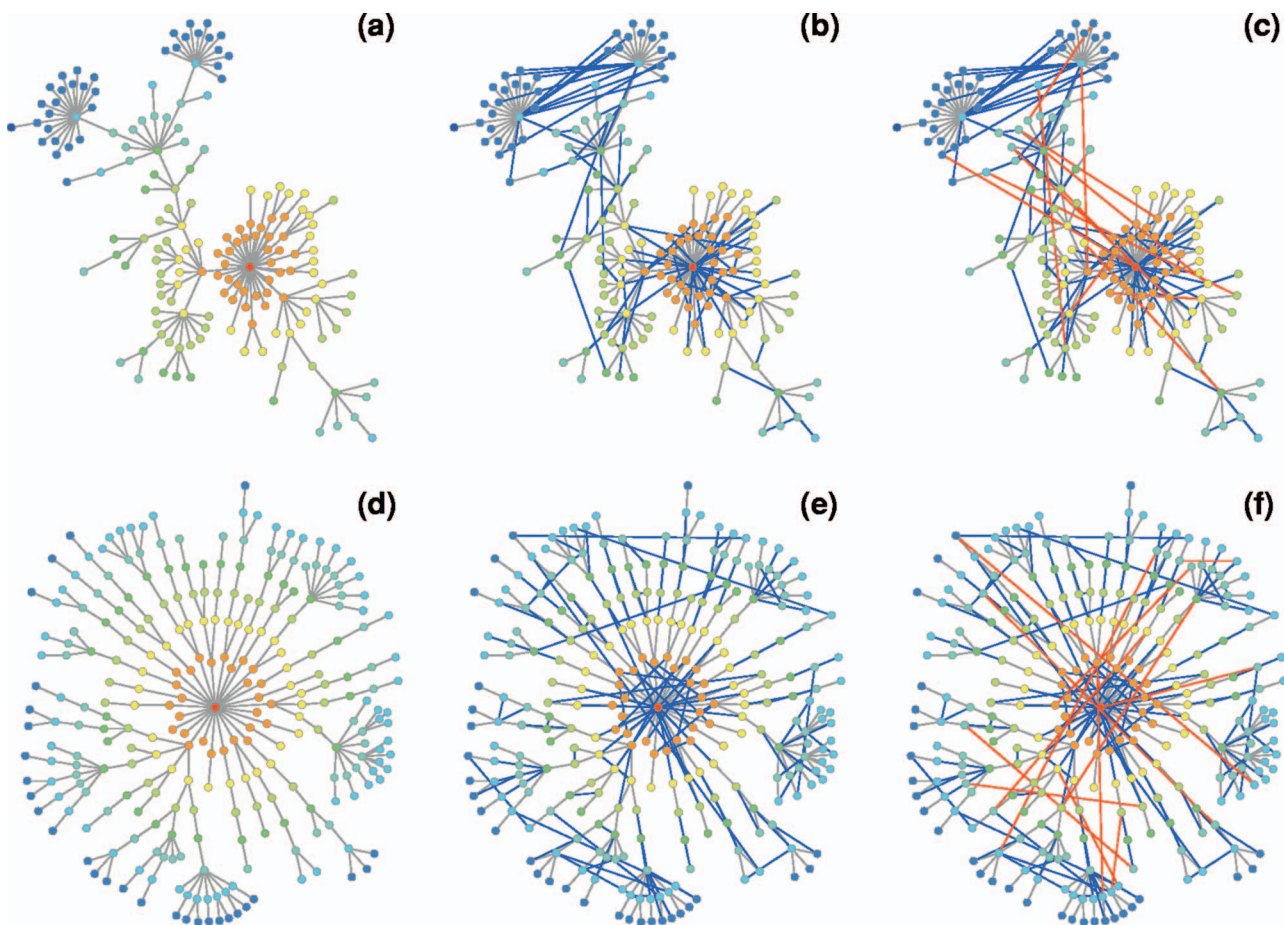
FIG. 6. (Color) Snapshots of the fractal network models. (a) A critical branching tree with $\gamma=2.3$ and $N=164$ created in step (i). (b) A network created by adding local shortcuts (blue) following the rule (ii) to the branching tree in (a). Parameter $p=0.5$ is used. This network is still fractal. (c) A network created by adding global shortcuts (red) following the rule (iii) to the network in (b). Parameter $q=0.02$ is used. This network is no longer fractal, but small world. (d) A supercritical branching tree with mean branching number $\langle n \rangle=2$, which is fractal as well as small world. (e) A dressed network to network (d) by local shortcuts (blue) generated with $p=0.5$. The network is fractal as well as small world. (f) A network created by adding global shortcuts (red) to the network in (e). $q=0.02$ is used. In (a)–(f), the colors of each vertex represent distinct generations from the root.

former behavior [Figs. 5(a)–5(d)], while the nonfractal networks exhibit the latter [Figs. 5(e)–5(j)]. This indicates that the shortcuts in the fractal networks are mainly local. For the case of (g), even though the shortcut-length distribution of the Internet at the AS level exhibits a peak for the dataset of year 2004, the peak locates at a rather short distance. Also such a peak does not appear in the dataset of year 2000. So the Internet may be categorized into the first category. Classification of SF networks according to such patterns appears to be in agreement with that based on the load exponent [10,31]. Note that the former-type networks have the load exponent $\delta \approx 2.0$, but the latter-type networks have $\delta \approx 2.2$. Fractal networks belong to the former type, however, all networks belonging to the former type are not always fractal, because the causal-tree network has also $\delta=2.0$, but it is not fractal. The Internet at the AS level and the BA tree are good such examples.

V. FRACTAL NETWORK MODEL

The observation of a plateau in the MBN for the skeleton of the fractal networks prompted the construction of a fractal network model based on a random branching tree. We construct the model by reversing the steps, followed thus far to reveal the fractality. We first construct a branching tree in which the branching proceeds stochastically with a prescribed branching probability b_n. We choose b_n to follow a power law with respect to n in order to generate a SF network. Then, the branching tree is dressed with local shortcuts as well as global ones. The global connection is introduced to observe the crossover from fractal to nonfractal behavior. The frequency of global shortcuts is an important parameter of the model. More specifically, we consider the branching probability b_n, i.e., the probability to generate n offsprings in each branching step, as

$$b_n = \frac{1}{Z}n^{-\gamma} \quad (\gamma > 2) \tag{8}$$

for $n \geq 1$, and

$$b_0 = 1 - \sum_{n=1}^{\infty} b_n \qquad (9)$$

for $n=0$. Then, the resulting tree network is a SF network with the degree exponent γ. In order to generate a *critical* branching tree, the normalization constant Z is set to be $Z = \zeta(\gamma-1)$, where $\zeta(x)$ is the Riemann zeta function, which follows from the criticality condition $\langle n \rangle = \Sigma_n n b_n = 1$. We can also generate a *supercritical* branching tree by setting $Z = \zeta(\gamma-1)/\langle n \rangle$ with $\langle n \rangle > 1$.

After we generate a branching tree, we dress it with shortcuts by increasing the degree of each vertex by a factor p and establishing the available connections between vertices. This can be achieved either in a local or global manner. An additional parameter q is introduced to describe the frequency of global shortcuts in the network. The creation rule of the fractal network model is described as follows:

(i) We start with a seed vertex from which n offsprings are stochastically generated with probability b_n $(n=0,\ldots,N-1)$. Each offspring then generates n branches with probability b_n. This process is repeated until we obtain a network of desired size N. If the growth of the tree stops before attaining size N, we restart the branching procedure.

(ii) Degree k_i of each vertex i is increased by a factor p such that vertex i obtains additional pk_i stubs for forming edges. From these stubs, qpk_i stubs are assigned to global shortcuts, while the remaining $(1-q)pk_i$ stubs are assigned to local shortcuts. In order to establish local shortcuts, we search vertices from the root. A vertex i that has at least one stub for local shortcuts is selected. Then, its connection partner is selected from the closest vertices from the vertex i to a vertex j, having available stubs for local shortcuts and not yet connected to i, to form an edge between i and j. This process is repeated until all the stubs for local shortcuts are linked.

(iii) Next, we choose two vertices i and j randomly, each of which has at least one stub for global shortcuts. We then connect them to form an edge if they are not already connected. This process is repeated until all stubs for global shortcuts are linked. This step is similar to the process used in the configuration model [32].

Network configurations obtained by the model with $\gamma = 2.3$ and $N=164$ are shown in Fig. 6. A critical branching tree with $\langle n \rangle = 1$ is shown in Fig. 6(a); this tree is dressed by local shortcuts [Fig. 6(b)] generated with $p=0.5$ and $q=0$ and both local and global shortcuts [Fig. 6(c)] with $p=0.5$ and $q=0.02$. A supercritical branching tree with $\langle n \rangle = 2$ is shown in Fig. 6(d); this tree is dressed by both local and global shortcuts generated with parameters $p=0.5$ and $q=0.02$ in Figs. 6(e) and 6(f), respectively.

We examine the fractal scaling in the network model and the MBN for its skeleton. In the case of a network generated from a critical branching tree (with $\gamma = 2.3$ and $N \approx 3 \times 10^5$) and dressed only by local shortcuts (with $p=0.5$ and $q=0$), 76% of all edges of the original branching tree are maintained in the skeleton. The branching tree and the dressed network exhibit fractal scalings with the same fractal exponent $d_B \approx 3.2$ [Fig. 7(a)]. This value appears to differ from
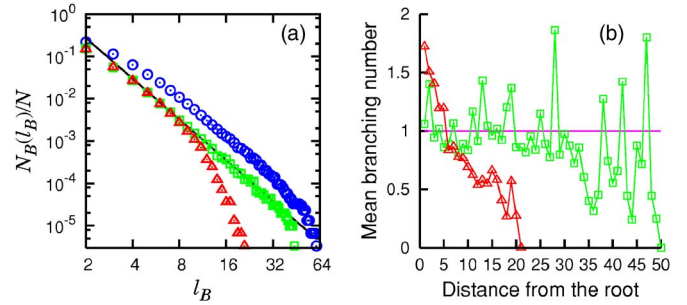

FIG. 7. (Color online) Fractal scaling analysis (a) and mean branching number (b) for the fractal models based on the critical branching tree with only local shortcuts with $p=0.5$ and $q=0$ ($\square$), and with 1% of global shortcuts with $p=0.5$ and $q=0.01$ ($\triangle$). The bare critical branching tree is represented by ($\bigcirc$). The solid line in (a) is guideline with a slope of -3.2. The measured degree exponent is $\gamma \approx 2.4$ and system size is $N=3 \times 10^5$.

the theoretical value ≈ 4.3 estimated from the formula (5). However, we notice that the measured value of the degree exponent of the *dressed* network is rather close to $\gamma = 2.4$, although the branching tree is generated with parameter $\gamma = 2.3$. This deviation roots from the stochastic process of dressing the branching tree by local edges. Thus, the expected value is $d_B = 3.5$. Therefore, the numerical deviation can be explained. The MBN of the skeleton of the dressed network displays a plateau around 1 [Fig. 7(b)]. Moreover, when we introduce 1% of global shortcuts ($p=0.5$ and $q=0.01$) to the critical branching tree, the box number $N_B(\ell_B)$ decays faster than any power law for large values of ℓ_B [Fig. 7(a)]; thus fractality is lost. Accordingly, in this case, the MBN of the skeleton decays to zero without a plateau [Fig. 7(b)]. The critical value q_c above which the network becomes nonfractal depends on the degree exponent γ, system size N, and number of shortcuts p. A more detailed analysis on this crossover behavior will be presented elsewhere [33].

The same analysis is performed for the model based on the supercritical branching tree with $\langle n \rangle = 2$ (Fig. 8). This tree with $\gamma = 2.3$ displays a power-law fractal scaling with fractal exponent $d_B \approx 4.2$ [Fig. 8(a)]; however, its MBN fluctuates heavily on and off about the expected value $\bar{n} = 2$, while exhibiting persistent branching [Fig. 8(b)]. Such a highly fluctuating MBN is similar to that observed in the skeleton of the WWW or the metabolic network [Figs. 3(a')–3(b')]. When dressed only by local shortcuts ($p=0.5$ and $q=0$), the dressed network still exhibits a power-law fractal scaling [Fig. 8(a)]. The MBN of its skeleton still exhibits large fluctuations [Fig. 8(b)]; however, its mean $\bar{n}$ decreases from 2. With 1% of global shortcuts ($q=0.01$), the fractal scaling exhibits a power-law behavior but with an exponential cutoff [Fig. 8(c)]. Interestingly, the MBN of its skeleton displays a plateau located around 1 with reduced fluctuations [Fig. 8(d)]. When we further increase the number of global shortcuts to 2% ($q=0.02$), the MBN of the skeleton decays without a plateau, and the network is no longer a fractal [Figs. 8(c) and 8(d)].

The fractal network model studied here is a generalization of the previous model [9] generated by including the supercritical branching case. Using this model, we can reproduce
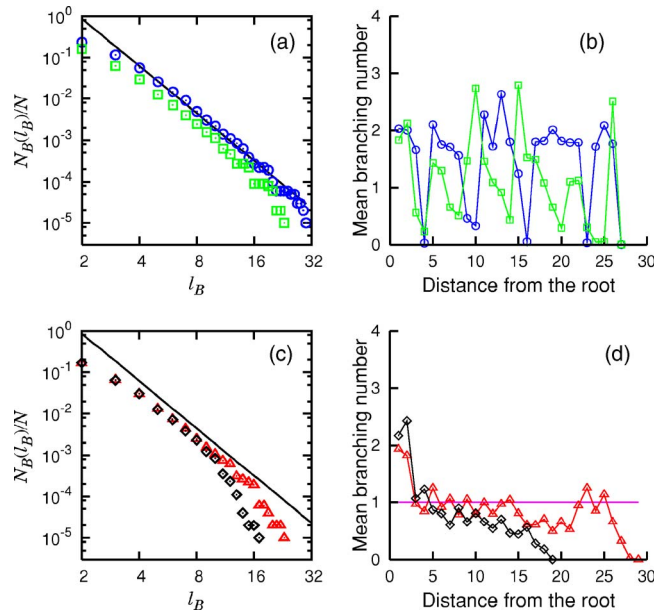
FIG. 8. (Color online) Fractal scaling analysis (a) and (c), and mean branching number (b) and (d) for the fractal models generated from a *supercritical* branching tree with $\langle n \rangle = 2$, dressed by short-cuts. The data are for the bare supercritical tree ($\bigcirc$) and dressed networks with $p=0.5$ and $q=0$ ($\square$), $p=0.5$ and $q=0.01$ ($\triangle$), and $p=0$ and $q=0.05$ ($\diamond$). The solid lines in (a) and (c) are guidelines with slopes of -4.2 each. The degree exponent is $\gamma = 2.3$ and system size is $N = 1 \times 10^5$.

the highly fluctuating behavior in the MBN observed in the WWW as well as the fractal scaling. We will also show that this generalization of the supercritical branching facilitates a better understanding of how the SW and fractal scaling coexist and do not contradict each other in such systems. In the following, we investigate the properties of the fractal network using the fractal network model as well as the real-world fractal networks.

VI. SMALL WORLDNESS AND BOX MASS DISTRIBUTION

In this section, we study the average box mass $\langle M(\ell) \rangle$ as a function of box size ℓ. The box mass is measured using two methods, the cluster-growing method and the box-covering method [1]. In the cluster-growing method, the box mass is defined as the number of vertices at a distance not greater than ℓ_C from a given vertex. Note that in the cluster-growing method, a vertex can be counted by more than one box, whereas in the box-covering method, it is counted only once. The cluster-growing method provides information on the SW of the network. The average box mass for the *critical* branching tree grows with distance ℓ_C, according to a power law with the exponent d_B,

$$\langle M_C(\ell_C) \rangle \sim \ell_C^{d_B}, \tag{10}$$

where d_B is defined in Eq. (5); this implies that the critical branching tree is a fractal. For the supercritical branching tree, the average mass grows exponentially with increase in distance ℓ_C,

$$\langle M_C(\ell_C) \rangle \sim \langle n \rangle^{\ell_C}. \tag{11}$$

This relation is equivalent to Eq. (3), thereby suggesting that the supercritical branching tree is a small-world network. On the other hand, the average box mass in the box-covering method is determined by the fractality. Since both the critical and supercritical branching trees are fractals, their box mass increases according to a power law. Thus, the analysis of the average box mass in the two methods will provide an insight into the interplay between SW and fractality.

We also consider the distribution of box masses $P_m(M)$ for each method. It is known [1] that in the cluster-growing method, the box mass distribution exhibits a peak at a characteristic mass, while it exhibits a fat tail without a peak in the box-covering method. However, the origin of the power-law behavior of the box mass distribution for the fractal networks has not been understood clearly. Here, we present a detailed analysis of the box mass distribution, showing that the exponent of the power-law behavior depends on the lateral size of the box. When the lateral size of the box is large, the exponent of the box mass distribution can be understood from the perspective of branching dynamics.

A. Real-world fractal networks

We first examine the average box mass $\langle M_C(\ell_C) \rangle$ in the cluster-growing method for the original network and the skeleton of each real-world fractal network. For the WWW, we find that both the original network and the skeleton exhibit an exponential increase in average box mass with distance ℓ_C [Fig. 9(a)]. Thus, the WWW is a small-world network and the skeleton of the WWW is a *supercritical* branching tree. For the metabolic network, while the original network is small world with Eq. (11), its skeleton appears to follow a power law, Eq. (10) [Fig. 9(b)]. Thus, the skeleton of the metabolic network is better described by a critical branching tree, although the original network is small world. The difference between the metabolic network and its skeleton probably originates from the presence of core subnetworks in the metabolic network, wherein the vertices are tightly interwoven through multiple pathways but are simplified into a tree in the skeleton [31,34,35]. On the other hand, for the protein interaction networks, both the original networks and the skeletons behave according to a power-law form of Eq. (10). Therefore, the protein interaction networks are not likely to be small world and their skeletons can be regarded as critical branching trees [Figs. 9(c) and 9(d)].

Next, we study the average box mass $\langle M_B(\ell_B) \rangle$ in the box-covering method. For the fractal networks and their skeletons, the average mass $\langle M_B(\ell_B) \rangle$ increases according to a power law with respect to box size ℓ_B of Eq. (2), regardless of whether it is critical or supercritical in the cluster-growing method as shown in Fig. 10. The fractal dimensions measured using the formula (2) are $d_B = 4.10 \pm 0.12, 3.53 \pm 0.12, 2.24 \pm 0.10,$ and 2.03 ± 0.05 for the WWW (a), metabolic network (b), protein interaction network of *H. sapiens* (c), and *S. cerevisiae* (d), respectively. These values are comparable to the ones obtained from the fractal scaling (1), which are $d_B = 4.10 \pm 0.12, 3.53 \pm 0.12,$
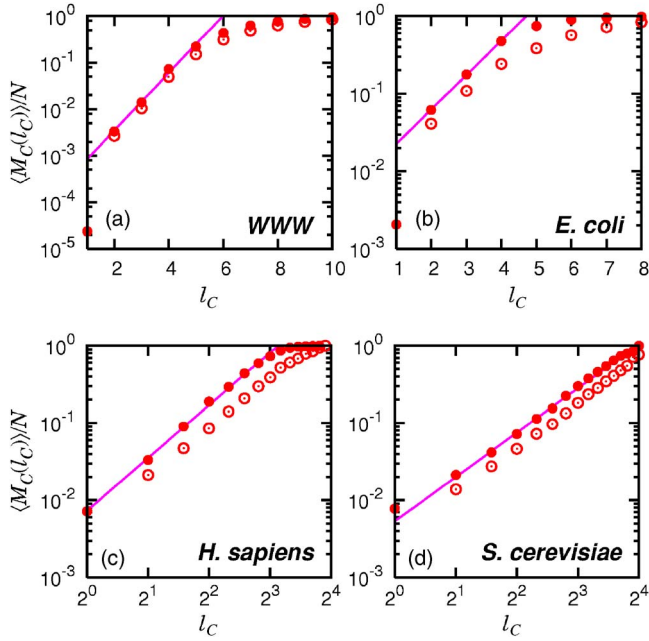
FIG. 9. (Color online) Average box mass $\langle M_C(\ell_C)\rangle$ in the cluster-growing method divided by the total number of vertices N, as a function of the distance ℓ_C. Plots of (a) and (b) are drawn on a semilogarithmic scale and those of (c) and (d) on a double-logarithmic scale, respectively. Filled and open symbols represent the original network and the skeleton of each network, respectively. The solid lines for reference in (c) and (d) have slopes of 1.9 and 2.3, respectively.
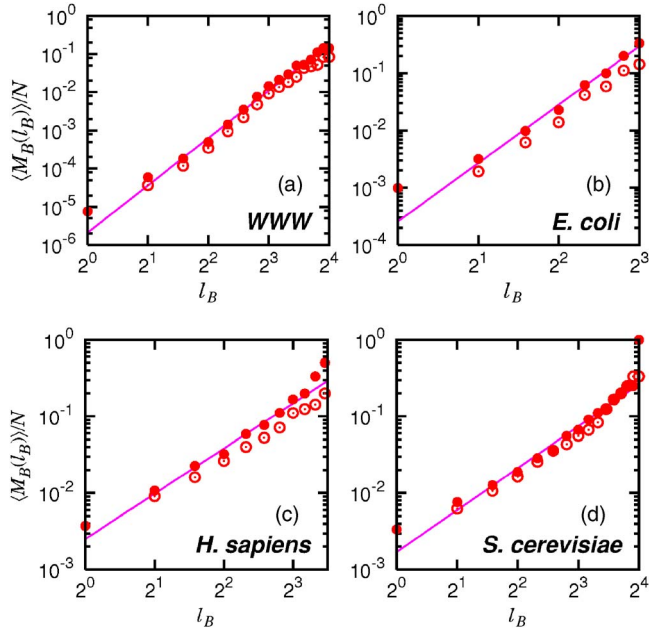

FIG. 10. (Color online) Average box mass $\langle M_B(\ell_B)\rangle$ divided by the total number of vertices N, as a function of box size ℓ_B in the box-covering method. Filled and open symbols represent the original network and the skeleton of each network, respectively. The solid lines (drawn for reference) have slopes of 4.10, 3.53, 2.24, and 2.03 for (a), (b), (c), and (d), respectively.

TABLE II. Behavior of the average box mass of the fractal networks and their skeletons in the cluster-growing and box-covering methods. * Due to finite-size effect, the characterization is based on limited data.

	Cluster-growing method	Box-covering method
World Wide Web	Exponential	Power law
World Wide Web (skeleton)	Exponential	Power law
Metabolic network*	Exponential	Power law
Metabolic network (skeleton)*	Power law	Power law
PIN of *H. sapiens*	Power law	Power law
PIN of *H. sapiens* (skeleton)	Power law	Power law
PIN of *S. cerevisiae*	Power law	Power law
PIN of *S. cerevisiae* (skeleton)	Power law	Power law

2.28±0.11, and 2.01±0.15 for (a), (b), (c), and (d), respectively. The results of the average box mass for the real-world fractal networks are summarized in Table II. Nonfractal networks exhibit the exponential relationship

$$\langle M_B(\ell_B)\rangle \sim \exp(\ell_B/\ell_0) \tag{12}$$

with a constant ℓ_0.

The different behaviors of the average mass in the two methods, the cluster-growing and box-covering methods, originate from whether overlap between the boxes is allowed. Thus, studying the extent of overlap of the boxes during the tiling can provide important information. In this regard, we measure the cumulative fraction $F_c(f)$ of vertices counted f times or more in the cluster-growing method for the WWW in Fig. 11. The cumulative fraction $F_c(f)$ is likely to follow a power law for small f, thereby indicating that the overlaps occur in a non-negligible frequency even for a small distance ℓ_C. The associated exponent decreases with increase in box size ℓ_C as the chances of overlaps increase. However, for large values of f, the large fraction of vertices counted
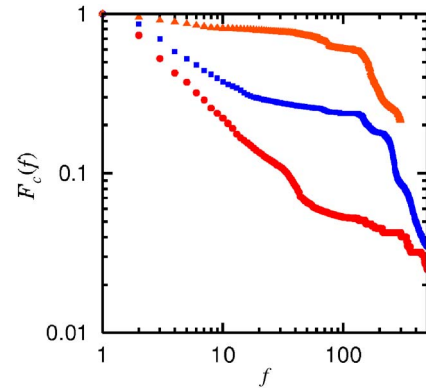

FIG. 11. (Color online) Cumulative fraction $F_c(f)$ of the vertices counted f times in the cluster-growing algorithm. $F_c(f)$ follows a power law in the small f region, where the slope depends on box size ℓ_C. However, for large values of f, the data largely deviate from the value extrapolated from the power-law behavior. Data are presented for $\ell_C=2$ (●), $\ell_C=3$ (■), and $\ell_C=5$ (▲).
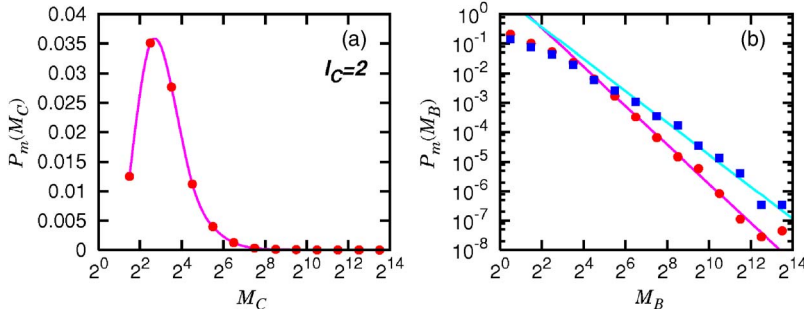
FIG. 12. (Color online) Box mass distribution in the cluster-growing method (a) and box-covering method (b) for the WWW. Data in (a) are for $\ell_C=2$ and those in (b) are for $\ell_B=2$ ($\bullet$) and $\ell_B=5$ ($\blacksquare$). The solid lines are guidelines with slopes of -2.2 and -1.8, respectively.

exceed the frequency extrapolated from the power-law behavior. As opposed to a bounded distribution such as a Poisson-type distribution, the broad distribution of f implies that a significant fraction of vertices are counted more than once in the cluster-growing method. Such multiple counting due to overlap is excluded in the box-covering method. Due to this exclusion effect, the mass of a box in the box-covering method is significantly lower than that in the cluster-growing method.

We study the box mass distributions in the two methods. As shown in Ref. [1], for the WWW, the box mass distribution in the cluster-growing method exhibits a clear peak [Fig. 12(a)]; on the other hand, in the box-covering method, it exhibits a fat tail, following an asymptotic power law,

$$P_m(M_B) \sim M_B^{-\eta} \quad (13)$$

[Fig. 12(b)]. We find that the exponent η depends on the box size ℓ_B. For small $\ell_B=1$ or 2, it is found that η is equal to γ; however, as ℓ_B increases, η approaches the exponent τ of the cluster-size distribution (7). This can be understood as follows. For small values of ℓ_B, the branching has not proceeded sufficiently to exhibit asymptotic behavior; thus, the box mass will simply scale with the degree of the seed vertex, which is selected randomly, yielding $\eta=\gamma$. This is most evident for $\ell_B=1$. On the other hand, as ℓ_B increases, the box grows and its size governs the scaling. The growth of the box can be approximated by the SF branching tree with the exponent γ, the size distribution of which follows a power law with the exponent τ given by Eq. (7), yielding $\eta=\tau$ for large ℓ_B. The numerical estimates of η obtained from the WWW are in reasonable agreement with the prediction as $\eta=\gamma \approx 2.3$ for $\ell_B=2$ and $\eta \approx 1.8$ for $\ell_B=5$ (Fig. 12).

B. Fractal network model

Here, we perform a similar analysis of the average box mass and the box mass distribution for the fractal network model introduced in Sec. V. We first consider a network model based on a *critical* branching tree with mean branching number $\langle n \rangle = 1$. For simplicity, we fix the parameters to be $\gamma=2.3$, $N=3 \times 10^5$, and $p=0.5$, while varying parameter q. When q is sufficiently small, i.e., $q \leq 0.001$, the model network exhibits a power-law scaling both in the cluster-growing method Eq. (10) and the box-covering method Eq. (2). The network thus remains as a fractal. However, for larger values of q like 0.01, the fractal scaling breaks down and the average box mass increases exponentially as Eq. (11) in both methods (Fig. 13), i.e., the network becomes small world.

The behavior of the average box mass of the fractal model network based on the supercritical tree is interesting. Once a supercritical tree is generated, the model network is dressed by local shortcuts with $p=0.5$. Then it simultaneously exhibits both an exponential increase in box mass in the cluster-growing method and a power-law increase in the box-covering method, as observed in the WWW. This coexistence persists when we introduce global shortcuts up to $q=0.01$ (Fig. 14). If we further increase q, the average box mass increases exponentially in both methods as the network loses fractality. Thus, the model network with supercritical branching tree and an appropriate number of local shortcuts can reproduce the small-world property of the average box mass function as well as the fractality.

Next, we study the box mass distribution for the fractal network model. We restart the analysis with the model network based on the critical branching tree with parameters $\gamma=2.3$, $N=3 \times 10^5$, and $p=0.5$. As with the real-world fractal networks like the WWW, the box mass distribution for the
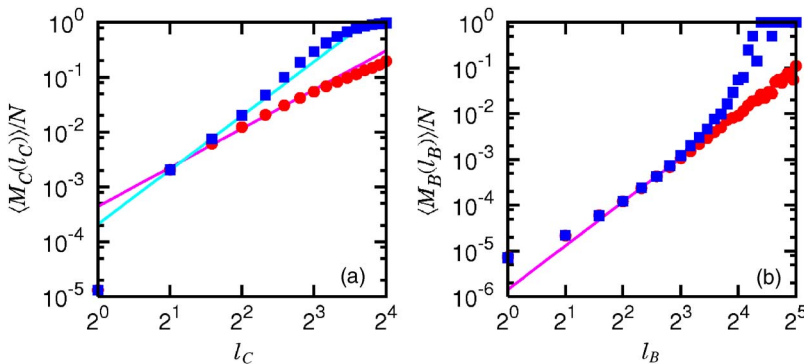

FIG. 13. (Color online) Average box mass versus box lateral size in the cluster-growing method (a) and the box-covering method (b) for the fractal network model constructed from a *critical* branching tree, dressed by shortcuts with $p=0.5$ and $q=0$ ($\bullet$) and $p=0.5$ and $q=0.01$ ($\blacksquare$). Degree exponent is $\gamma=2.3$ and system size is $N=3 \times 10^5$. Solid lines in (a) have slopes of 3.3 and 2.4, respectively, and the solid line in (b) has a slope of 3.3.
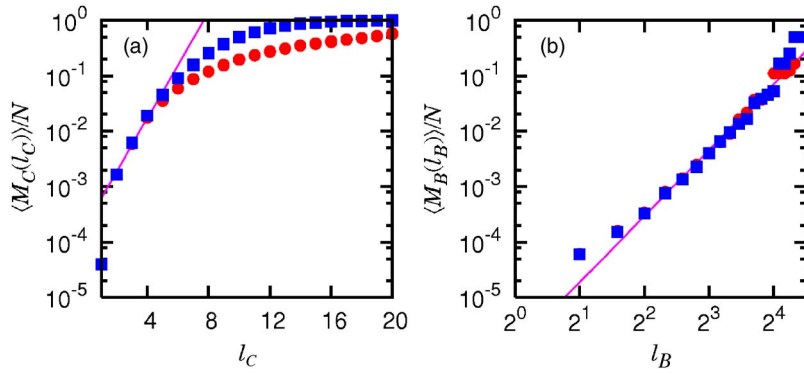
FIG. 14. (Color online) Average box mass as a function of box size in the cluster-growing method (a) and the box-covering method (b) for the model network constructed from a *supercritical* branching tree, dressed by shortcuts with $p=0.5$ and $q=0$ (●) and $p=0.5$ and $q=0.01$ (■). Degree exponent is $\gamma=2.3$, and system size $N=1\times10^5$. The solid line in (b) has a slope of 4.0, which is drawn for guidance.
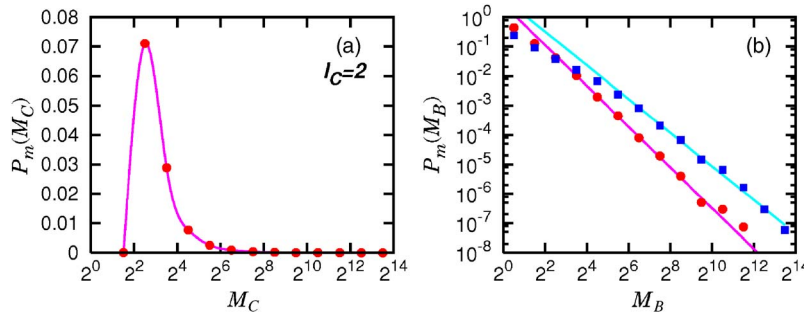

FIG. 15. (Color online) Box mass distribution in the cluster-growing method (a) and box-covering method (b) for the fractal model network grown from a *critical* branching tree with $\gamma=2.3$ and dressed by shortcuts generated with $p=0.5$ and $q=0.001$. The data in (b) are for $\ell_B=2$ (●) and $\ell_B=5$ (■). Their slopes are -2.3 and -1.8, respectively. The system size is $N\approx3\times10^5$.
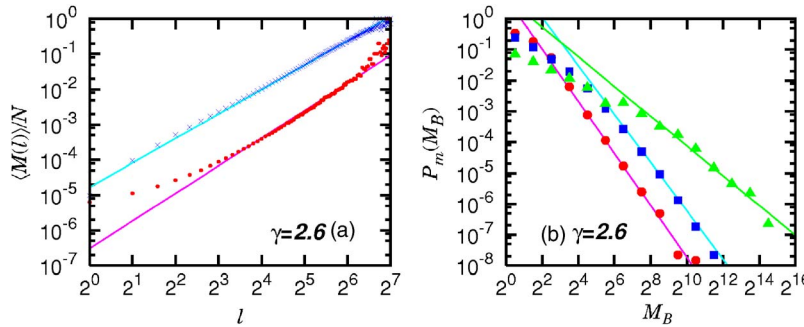

FIG. 16. (Color online) (a) Average box mass versus box size in the cluster-growing (×) and box-covering (■) methods for a bare critical branching tree with $\gamma=2.6$. Solid lines, drawn for guidance, have slopes of 2.3 (×) and 2.6 (■), respectively. (b) Box mass distribution for the bare tree of (a). Solid guidelines have slopes of -2.8 for $\ell_B=2$ (●), -2.6 for $\ell_B=5$ (■), and -1.6 for $\ell_B=32$ (▲).
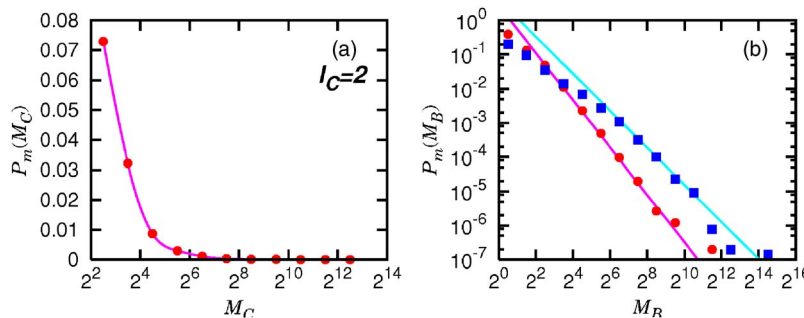

FIG. 17. (Color online) Box mass distribution in the cluster-growing method (a) and box-covering method (b) for the fractal model network grown from a supercritical branching tree with $\langle n\rangle=2$ and $\gamma=2.3$, which is dressed by shortcuts with the parameters $p=0.5$ and $q=0$. The box size in (b) is $\ell_M=2$ (●) and $\ell_M=5$ (■). Solid lines in (b) have slopes -2.3 and -1.8, drawn for guidance. The system size is $N\approx1\times10^5$.
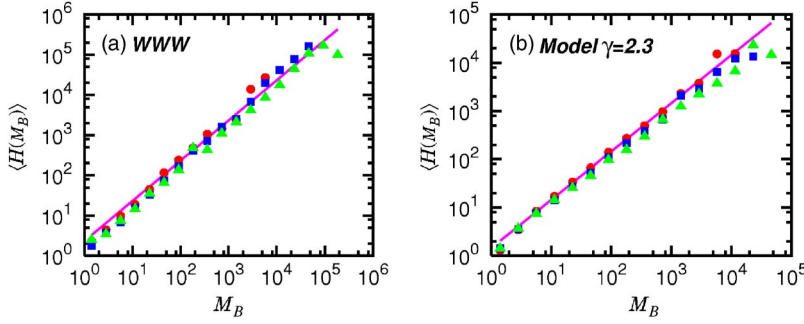
FIG. 18. (Color online) Plot of the average perimeter $\langle H(M_B) \rangle$ versus box mass M_B for the WWW (a) and the model network with the parameters of $\gamma=2.3$, $p=0.5$, and $q=0.0$ (b). Data are for box sizes $\ell_B=2$ (●), $\ell_B=3$ (■), $\ell_B=5$ (▲). The solid line (drawn as reference) has a slope of 1.0 for both (a) and (b).

model network exhibits a peak at a finite mass in the cluster-growing method. The box mass distribution in the box-covering method follows an asymptotic power law with exponent η. As observed for the WWW, we observe that the exponent η depends on the box size. For $q=0.001$, it is found that $\eta \approx 2.3$ for small $\ell_B=2$, and $\eta \approx 1.8$ for large $\ell_B=5$ (Fig. 15). The latter value $\eta \approx 1.8$ is in agreement with $\tau=\gamma/(\gamma-1) \approx 1.8$ from Eq. (7). Such ℓ_B-dependent behavior of the box mass distribution can also be observed for another value of γ, for example, $\gamma=2.6$ (Fig. 16). In such cases, the behavior $\eta=\tau$ appears for large values of ℓ_B, for example, $\ell_B=32$ for $\gamma=2.6$.

Next, when the model network is constructed based on a supercritical branching tree (with $\gamma=2.3$ and $\langle n \rangle=2$) and is dressed by shortcuts (with $p=0.5$ and $q=0.001$), $\eta \approx 2.3$ is measured for $\ell_B=2$, however, $\eta \approx 1.8$ for $\ell_B=5$ (Fig. 17). The obtained value $\eta \approx 1.8$ is again in agreement with the expected value $\tau \approx 1.8$ for $\gamma=2.3$.

VII. PERIMETER OF A BOX

The boundary of a fractal object is an important physical quantity and is considered to be another fractal object. For example, the area of the spin domain of the Ising model at critical temperature, which corresponds to magnetization, is a fractal object, and the interface length of the spin domain is another fractal object, corresponding to the singular part of internal energy [36]. Moreover, a percolation cluster is a fractal object and its outer boundary, referred to as "hull," is also a fractal [37,38].

We define the perimeter H_α of a given box α as the number of edges connected on one end to the vertices within the box α and on the other end to the vertices in other boxes. The perimeter H_α is examined as a function of the box mass $M_{B,\alpha}$ of the box α. Then, we can define the average perimeter $\langle H(M_B) \rangle$ over the boxes with box mass M_B. We find that the following power-law relationship exists,

$$\langle H(M_B) \rangle \sim M_B^{d_H/d_B}. \tag{14}$$

The new exponent d_H (the hull exponent for the fractal network) is analogous to the one used in the percolation theory [37,38].

The power-law relation (14) is tested for the WWW and the network model generated with $\gamma=2.3$ and $\langle n \rangle=1$. It appears that $\langle H(M_B) \rangle$ depends on the box mass M_B linearly, i.e., $d_H/d_B \approx 1$, irrespective of ℓ_B for the WWW [Fig. 18(a)];

however, it depends on ℓ_B weakly for the fractal network model. For $\ell_B=2$ and 3, $d_H/d_B \approx 1$; however, for $\ell_B=5$, d_H/d_B is likely to be marginally smaller than 1 [Fig. 18(b)]. The linear behavior implies $d_H=d_B$, and is observed in the connections between the percolation clusters near the critical point for SF networks [39].

VIII. CONCLUSIONS

Recently, it was shown that some SF networks exhibit fractal scaling, $N_B(\ell_B) \sim \ell_B^{-d_B}$, where $N_B(\ell_B)$ is the number of boxes needed to tile the entire network with boxes of size ℓ_B. In this paper, we have introduced a modified version of the box-covering method, which makes implementation easy. The origin of fractal scaling is understood from the perspective of criticality and supercriticality of the skeleton embedded underneath each fractal SF network. By performing the analysis of the average box mass as a function of the box size for the box-covering and cluster-growing methods, and the mean branching number as a function of the distance from the root, we found that the skeleton of the WWW is a super-critical branching tree, while the skeletons of other biological networks such as the metabolic network of *E. coli* and the protein interaction networks of *H. sapiens* and *S. cerevisiae* are critical branching trees. Based on this observation, we constructed the fractal network model. The box mass is heterogeneous and they exhibit a fat-tailed behavior, $P_m(M) \sim M^{-\eta}$. We found that the exponent η depends on the lateral size ℓ_B of the box. When ℓ_B is small, η is equal to the degree exponent γ; on the other hand, as ℓ_B increases, η approaches the exponent $\tau=\gamma/(\gamma-1)$ for the cluster-size distribution of the branching tree; this can be predicted from the skeleton. Finally, we studied the number of edges that interconnect a given box and other boxes, forming the perimeter of a box, as a function of the box mass. It appears that the perimeter depends on the box mass linearly, and the perimeter exponent is equal to the fractal dimension.

[1] C. Song, S. Havlin, and H. A. Makse, Nature (London) **433**, 392 (2005).

[2] R. Albert, H. Jeong, and A.-L. Barabási, Nature (London) **401**, 130 (1999).

[3] H. Jeong, B. Tombor, R. Albert, Z. N. Oltvai, and A.-L. Barabási, Nature (London) **407**, 651 (2000).

[4] I. Xenarious *et al.*, Nucleic Acids Res. **28**, 289 (2000).

[5] A.-L. Barabási and R. Albert, Science **286**, 509 (1999).

[6] J. Feder, *Fractals* (Plenum, New York, 1988).

[7] S.-H. Yook, F. Radicchi, and H. Meyer-Ortmanns, Phys. Rev. E **72**, 045105(R) (2005).

[8] C. Song, S. Havlin, and H. A. Makse, Nat. Phys. **2**, 275 (2006).

[9] K.-I. Goh, G. Salvi, B. Kahng, and D. Kim, Phys. Rev. Lett. **96**, 018701 (2006).

[10] D.-H. Kim, J. D. Noh, and H. Jeong, Phys. Rev. E **70**, 046126 (2004).

[11] L. C. Freeman, Sociometry **40**, 35 (1977).

[12] M. Girvan and M. E. J. Newman, Proc. Natl. Acad. Sci. U.S.A. **99**, 7821 (2002).

[13] K.-I. Goh, B. Kahng, and D. Kim, Phys. Rev. Lett. **87**, 278701 (2001).

[14] T. E. Harris, *Theory of Branching Processes* (Springer-Verlag, Berlin, 1963).

[15] Z. Burda, J. D. Correia, and A. Krzywicki, Phys. Rev. E **64**, 046118 (2001).

[16] K.-I. Goh, D.-S. Lee, B. Kahng, and D. Kim, Phys. Rev. Lett. **91**, 148701 (2003).

[17] L. Donetti and C. Destri, J. Phys. A **37**, 6003 (2004).

[18] A. Saichev, A. Helmstetter, and D. Sornette, Pure Appl. Geophys. **162**, 1113 (2005).

[19] D.-S. Lee *et al.* (unpublished).

[20] The fractal scaling of the protein interaction network for *S. cerevisiae* behaves differently depending on the dataset. The dataset we use is from J.-D. Han *et al.*, Nature (London) **430**, 88 (2004).

[21] Internet Movie Database, http://imdb.com/

[22] M. E. J. Newman, Proc. Natl. Acad. Sci. U.S.A. **98**, 404 (2001).

[23] University of Oregon Route Views Archive Project, http://archive.routeviews.org/

[24] SCAN project, http://www.isi.edu/scan/scan.html

[25] D. J. Watts and S. H. Strogatz, Nature (London) **393**, 440 (1998).

[26] L. A. Braunstein, S. V. Buldyrev, R. Cohen, S. Havlin, and H. E. Stanley, Phys. Rev. Lett. **91**, 168701 (2003).

[27] R. Cohen *et al.*, in *Handbook of Graphs and Networks*, edited by S. Bornholdt and H. G. Schuster (Wiley-VCH, New York, 2002), Chap. 4.

[28] S. Jung, S. Kim, and B. Kahng, Phys. Rev. E **65**, 056101 (2002).

[29] E. Ravasz and A.-L. Barabási, Phys. Rev. E **67**, 026112 (2003).

[30] P. Bialas, Z. Burda, J. Jurkiewicz, and A. Krzywicki, Phys. Rev. E **67**, 066106 (2003).

[31] K.-I. Goh, E. S. Oh, H. Jeong, B. Kahng, and D. Kim, Proc. Natl. Acad. Sci. U.S.A. **99**, 12583 (2002).

[32] M. Molloy and B. Reed, Random Struct. Algorithms **6**, 161 (1995).

[33] J. S. Kim *et al.* (unpublished).

[34] E. Almaas, B. Kovacs, T. Vicsek, Z. N. Oltvai, and A.-L. Barabási, Nature (London) **427**, 839 (2004).

[35] C.-M. Ghim, K.-I. Goh, and B. Kahng, J. Theor. Biol. **237**, 401 (2005).

[36] M. den Nijs, Physica A **251**, 52 (1998).

[37] P. L. Leath and G. R. Reich, J. Phys. C **11**, 4017 (1978).

[38] R. F. Voss, J. Phys. A **17**, L373 (1984).

[39] S. Sreenivasan, T. Kalisky, L. A. Braunstein, S. V. Buldyrev, S. Havlin, and H. E. Stanley, Phys. Rev. E **70**, 046133 (2004).